
Transformer Alignment in Large Language Models

Murdock Aubry* Haoming Meng* Anton Sugolov* Vardan Papyan

University of Toronto

Abstract

Large Language Models (LLMs) have made significant strides in natural language processing, and a precise understanding of the internal mechanisms driving their success is essential. We regard LLMs as transforming embeddings via a discrete, coupled, nonlinear, dynamical system in high dimensions. This perspective motivates tracing the trajectories of individual tokens as they pass through transformer blocks, and linearizing the system along these trajectories through their Jacobian matrices. In our analysis of 38 openly available LLMs, we uncover the alignment of top left and right singular vectors of Residual Jacobians, as well as the emergence of linearity and layer-wise exponential growth. Notably, we discover that increased alignment *positively correlates* with model performance. Metrics evaluated post-training show significant improvement in comparison to measurements made with randomly initialized weights, highlighting the significant effects of training in transformers. These findings reveal a remarkable level of regularity that has previously been overlooked, reinforcing the dynamical interpretation and paving the way for deeper understanding and optimization of LLM architectures.

1 Introduction

Large language models (LLMs), as exemplified by BERT and GPT-series [Devlin et al., 2019, Brown et al., 2020], have revolutionized the field of natural language processing through their adoption of the transformer architecture [Vaswani et al., 2017]. Despite their widespread success, the internal mechanisms that underpin their performance are not fully understood.

Previous works viewed certain types of deep networks as implementing discrete, nonlinear dynamical systems, operating in high dimensions [Greff et al., 2016, Papyan et al., 2017, Ebski et al., 2018, Chen et al., 2018, Bai et al., 2019, Rothauge et al., 2019, Li and Papyan, 2023, Gai and Zhang, 2021, Haber and Ruthotto, 2017, Ee, 2017]. The term *discrete* reflects the network’s finite depth; *nonlinear* refers to the model’s nonlinear components; and *dynamical* is due to the residual connections spanning various layers. This motivates us to trace the dynamics of individual tokens as they traverse through the numerous transformer blocks, and to linearize the system through its Jacobian matrices.

1.1 Residual Alignment

Our investigation draws inspiration from a recent study by Li and Papyan [2023] on Residual Networks (ResNets) [He et al., 2016], which uncovered a phenomenon they termed Residual Alignment (RA), marked by several distinct characteristics in hidden representations of ResNets:

- (RA1) Linear and equispaced trajectories in layer-wise progression of intermediate representations.
- (RA2) Alignment of top left and right singular vectors in the linearizations of residual blocks.
- (RA3) The rank of Residual Jacobians is at most the number of classes.
- (RA4) Top singular values of Residual Jacobians scale inversely with depth.

*Equal Contribution

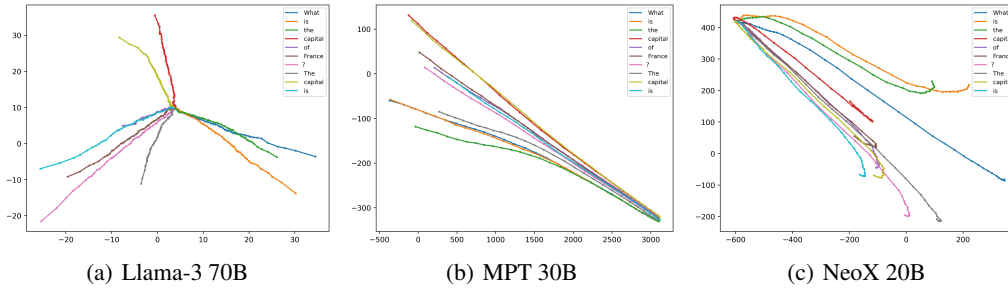


Figure 1: **Trajectories of Hidden Representations in LLMs.** Visualization of the layer-wise trajectories of hidden representations in Llama 3 70B, Mistral 30B, and NeoX 20B in the prompt: What is the capital of France? The capital is. Trajectories of tokens are plotted in latent space, visualized with a 2-dimension principal component projection. A clear directed and outward growth is visible in each token trajectory.

1.2 Contributions

We uncover Transformer Alignment (TA), characterized by two properties (analogous to those of RA) that consistently emerge with training in 38 openly available base and fine-tuned LLMs (Appendix A.1) including the Falcon [Almazrouei et al., 2023], Llama-3 [AI@Meta, 2024], Llama-2 [Touvron et al., 2023], MPT [Team, 2023a,b], Mistral v0.1 [Jiang et al., 2023], Gemma [Team et al., 2024], NeoX [Black et al., 2022], Neo [Black et al., 2021, Gao et al., 2020], and Pythia [Biderman et al., 2023] families. The properties are given by

- (TA1) Emergence of linearity and exponentially distanced trajectories of intermediate representations in layer-wise progression.
- (TA2) Alignment of top left and right singular vectors in the linearizations of transformer blocks through their Residual Jacobians.

Due to the large vocabulary size relative to the embedding size in LLMs, Residual Jacobians maintain rank of at most the vocabulary size, and so the previous (RA3) immediately holds. Further, trained LLMs do not exhibit a consistent inverse scaling of top singular values with depth, and scaling varies considerably between models, demonstrating a lack of (RA4). In contrast to ResNets, the layer-wise progression of transformer representations is better described with an exponential evolution, rather than an equispaced linear progression.

Additionally, we explore the relationship between (TA2) and generalization, and uncover that increased alignment of Residual Jacobian singular vectors **correlates** with improved Open LLM leaderboard [Beeching et al., 2023] **benchmark score** (Figure 3), raising valuable insight to the mathematical properties of LLM transformers and their connections to generalization.

2 Background on Large Language Models

In the input layer, $l = 0$, textual prompts undergo tokenization and are combined with positional encodings to create an initial high-dimensional embedding, denoted by $x_i^0 \in \mathbb{R}^{d_{\text{model}}}$ for the i^{th} token. When these embeddings are stacked together, they form a matrix:

$$X^0 = (x_1^0, x_2^0, \dots, x_n^0) \in \mathbb{R}^{d_{\text{model}} \times n}. \quad (1)$$

The embeddings then pass through L transformer blocks:

$$X^0 \xrightarrow{f_{\text{block}}^1} X^1 \xrightarrow{f_{\text{block}}^2} \dots X^{L-1} \xrightarrow{f_{\text{block}}^L} X^L. \quad (2)$$

Here, $X^l = f_{\text{block}}^l(X^{l-1})$ denotes the embeddings after the l^{th} block, consisting of causal multi-headed attention (MHA), a feed-forward network (FFN), and normalization layers (LN) with residual

connections:

$$h^{l+1}(X^l) = \text{MHA}(\text{LN}(X^l)) \quad (3)$$

$$g^{l+1}(X^l) = \text{LN}(X^l + h^{l+1}(X^l)) \quad (4)$$

$$f_{\text{block}}^{l+1}(X^l) = X^l + h^{l+1}(X^l) + \text{FFN}(g^{l+1}(X^l)), \quad (5)$$

where the MHA, LN, FFN are implicitly indexed by layer. In the final representation, an additional layer normalization is applied:

$$f_{\text{block}}^L(X^{L-1}) = \text{LN}(X^{L-1} + h^L(X^{L-1}) + \text{FFN}(g^L(X^{L-1}))). \quad (6)$$

The output X^L from the final block f^L is passed into a bias-free linear layer $M \in \mathbb{R}^{d_{\text{vocab}} \times d_{\text{model}}}$, with d_{vocab} denoting the size of the token vocabulary and d_{model} is the dimension of the token embeddings. This layer M computes final-layer logits for each token embedding, $\ell_i = Mx_i^L$. The prediction for the next token is then determined by selecting the maximal logit value: $\arg \max_{v \in \text{tokens}} \ell_{v,n}$.

3 Methods

3.1 Suite of Large Language Models

Our study evaluates a total of 38 LLMs (24 base LLMs and 14 fine-tuned, see Appendix A.1) that were independently trained by various individuals and organizations. These models, provided through HuggingFace [Wolf et al., 2020], vary in terms of parameter budgets, number of layers, hidden dimensions, and training tokens. A summary of the models under consideration is presented in Table 1 of Appendix A.1. Measurements are made for models with varying parameter sizes with GPUs satisfying appropriate memory requirements, further detailed in Appendix A.3.

3.2 Prompt Data

We evaluate these LLMs using prompts of varying length, ambiguity, and context, sourced from the test set of ARC [Clark et al., 2018], GSM8K [Cobbe et al., 2021], HellaSwag [Zellers et al., 2019], MMLU [Hendrycks et al., 2021], Truthful QA [Lin et al., 2022], and Winogrande [Sakaguchi et al., 2019]. These datasets set the performance benchmarks on the HuggingFace Open LLM Leaderboard [Beeching et al., 2023] since they encompass a diverse set of language tasks. Post-prompting, we assess the models using several metrics, detailed in the following subsections.

3.3 Alignment of Singular Vectors of Residual Jacobians

To demonstrate the presence of (TA2), we examine the properties of the transformer blocks and the relationships between them. This is done by analyzing the linearizations of the blocks given by their *Residual Jacobian* matrices

$$J_l^i = \frac{\partial}{\partial x_i^{l-1}} (h^l(X^{l-1}) + \text{FFN}_l(g^l(X^{l-1})))_i, \quad (7)$$

defined for each $l = 1, \dots, L$, and $i = 1, \dots, n$. Note that this is the Jacobian matrix for each transformer block without the contribution from the skip connection from the input of the block, analogous to the quantities measured by Li and Pappan [2023].

The singular value decompositions of these J_l^i are computed, i.e., $J_l^i = U_l S_l V_l^\top$ (with superscript i , indicating the token, omitted for clarity), where $U_l \in \mathbb{R}^{d_{\text{model}} \times d_{\text{model}}}$ and $V_l \in \mathbb{R}^{d_{\text{model}} \times d_{\text{model}}}$ are the matrices of left and right singular vectors respectively, and $S_l \in \mathbb{R}^{d_{\text{model}} \times d_{\text{model}}}$ is the singular value matrix.

The matrices $A_{i,j,K} := U_{j,K}^\top J_i V_{j,K}$ are plotted over all pairs of depths $i, j \in \{1, \dots, L\}$, where $U_{j,K}$ and $V_{j,K}$ are the sub-matrices with columns that are the top- K left and right singular vectors of J_j , respectively.

To quantify the misalignment of singular vectors of the Residual Jacobians at depths i and j , we measure how far the $A_{i,j,K}$ are from being diagonal. More precisely, we define the misalignment of $A_{i,j,K}$ as

$$m(A_{i,j,K}) = \|A_{i,j,K} - \text{Diag}(A_{i,j,K})\|_F, \quad (8)$$

where $\text{Diag}(A_{i,j,K})$ is the matrix $A_{i,j,K}$ with all non-diagonal entries replaced by zero and $\|\cdot\|_F$ denotes the Frobenius norm.

3.4 Layer-Wise Exponential Growth

To demonstrate the presence of **(TA1)**, we measure the *expodistance* of the hidden trajectories, defined below. In this context, each layer in the model corresponds to a unit time step of a dynamical system, so we denote $\dot{x}_i(t) = x_i(t+1) - x_i(t)$ the time derivative of the i^{th} token. Assuming exponential growth of the embedding norms as they flow through the hidden layers, we can write,

$$\|\dot{x}_i(t)\| \approx e^{\alpha t} \|\dot{x}_i(0)\| \quad (9)$$

for some fixed $\alpha \in \mathbb{R}$. We quantify the validity of the approximation in Equation (9) by measuring the coefficient of variation of α for each trajectory. Namely, following (9),

$$\alpha_t^i \approx \frac{1}{t} \ln \left(\frac{\|\dot{x}_i(t)\|}{\|\dot{x}_i(0)\|} \right) \quad (10)$$

for each time (layer) t and token i . Under exponential growth, it is expected that α_t^i is independent of time. We then denote the expodistance (ED) of the trajectory of the i^{th} token of a given sequence by

$$ED_i = \frac{\text{Var}_t \alpha_t^i}{(\text{Avg}_t \alpha_t^i)^2} \quad (11)$$

This measurement is motivated by the parametrization discussed in Appendix A.2 and serves as a method to test the validity of the linearization presented in Equation (15).

3.5 Linearity of Trajectories

Linearity in intermediate embeddings **(TA1)** is quantified with the *line-shape score* (LSS), defined by Gai and Zhang [2021] as

$$\text{LSS}_i^{0,\dots,L} = \frac{L}{\|\tilde{x}_i^L - \tilde{x}_i^0\|_2}, \quad (12)$$

where $\tilde{x}_i^0 = x_i^0$, i.e., the input embeddings passed to the LLM, and \tilde{x}_i^l is defined recursively as

$$\tilde{x}_i^l = \tilde{x}_i^{l-1} + \frac{x_i^l - x_i^{l-1}}{\|x_i^l - x_i^{l-1}\|_2} \quad \text{for } l = 1, \dots, L. \quad (13)$$

Note that $\text{LSS} \geq 1$, with $\text{LSS} = 1$ if and only if the intermediate representations x_i^0, \dots, x_i^L form a co-linear trajectory.

3.6 Visualization of Trajectories with PCA

Each token, with initial embedding x_i^0 , forms a trajectory $x_i^0, x_i^1, \dots, x_i^L$ as it passes through the L transformer blocks. The dynamics in high-dimensional space are visualized through a 2-dimensional principal component (PC) projection, PC_L , fitted to the last layer embeddings $X^L = (x_1^L, x_2^L, \dots, x_n^L)$. The projected embeddings, $\text{PC}_L(x_i^0), \text{PC}_L(x_i^1), \dots, \text{PC}_L(x_i^L)$, are plotted for each of the $i = 1, \dots, n$ trajectories.

4 Results

4.1 Alignment of Singular Vectors of Residual Jacobians

In trained LLMs, we observe **(TA2)**, that is, alignment of the top singular vectors of the Jacobians J_l across depth (Figure 2 bottom row), evident in the distinct diagonal lines present in the matrix subplots. This phenomenon is consistently observed across LLMs, similar to **(RA2)**, which was

observed by Li and Pappayan [2023] in ResNets. On the other hand, in untrained models (Figure 2 top row), there is no alignment between singular vectors of Residual Jacobians across different depths. There is alignment along the diagonal, however, because each Residual Jacobian is trivially diagonalized by its own singular vectors in $A_{i,j,K}$. This suggests that **(TA2)**, the alignment of singular vectors of Residual Jacobians, emerges through training.

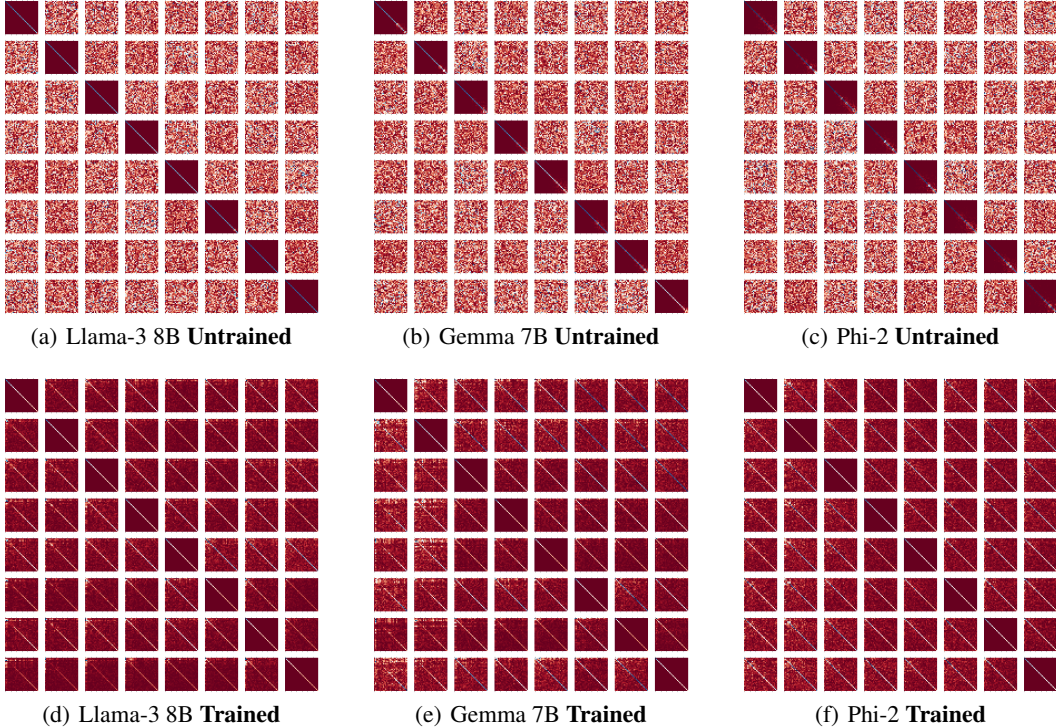


Figure 2: **(TA2): Residual Jacobian Alignment of Top Singular Vectors.** The figure illustrates the alignment of Residual Jacobians across transformer blocks 9 to 16. For each subplot, in the square located at entry (i, j) , the absolute values of the entries of matrices $A_{i,j,30} = U_{j,30}^\top J_i V_{j,30}$ (using the top 30 singular vectors) are visualized using the prompt ‘What is the capital of France? The capital is’, tracing the trajectory of its final token. The diagonal line in the trained plots (bottom row) indicates alignment of Residual Jacobians, where the top singular vectors of J_j diagonalize J_i . In the untrained models (top row), there is no alignment between singular vectors of Residual Jacobians across layer. Additional visualizations are included in Appendix A.4 (Figure 6)

To understand this phenomenon more precisely, for each LLM, we measure the average alignment (which we define to be negative misalignment) across prompts in the 6 evaluation datasets (Section 3.2), where for each prompt, the misalignment $m(A_{i,j,K})$ is averaged over layers $i, j = 1, \dots, L$. We plot the negative misalignment values against the benchmark scores across several LLMs (Figure 3). Our results reveal a consistent pattern: an increase in alignment corresponds to an increase in benchmark scores. This observation suggests a compelling relationship between stronger alignment of singular vectors of Residual Jacobians and improved generalization performance.

4.2 Linearity of Trajectories

We observe **(TA1)** in each LLM, evident in the LSS of layer-wise trajectories at initialization and after training evaluated over benchmark prompts (Figure 4), in agreement with **(RA1)** in ResNets. Linear and expansive dynamical behavior is demonstrated in Llama-3 70B, Mistral 30B, and NeoX 20B through low dimensional projections of embedding trajectories (Figure 1). The LSS of the trajectories has an average value 4.25 across trained models, while taking average values of 6.54 at initialization, and is evidenced by the low variation across benchmark prompts (Figure 4).

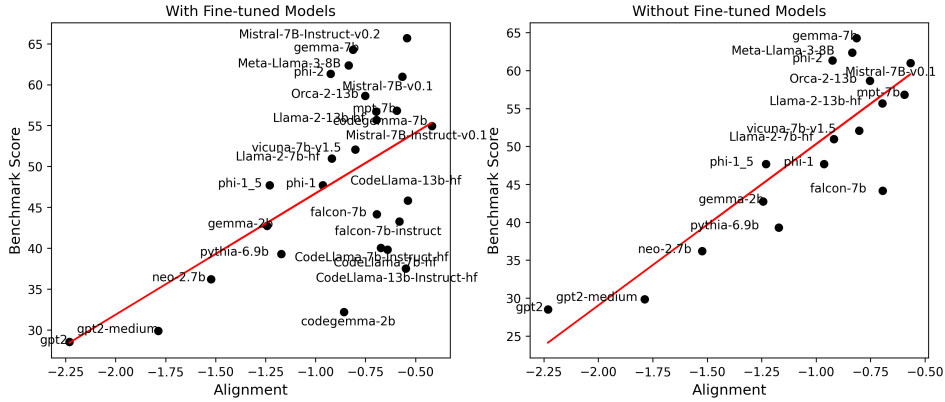


Figure 3: **Relationship between Alignment and Benchmark Score.** The plot illustrates the relationship between average alignment (negative misalignment) and benchmark score across various LLMs. The left subplot includes models fine-tuned for coding and instruction, while the right excludes these models. We make this distinction as these fine-tuned models are for code and instruction, rather than being fine-tuned on the benchmark tasks. The data shows a noticeable trend: increased alignment correlates with elevated benchmark scores. In particular, when excluding the code and instruction models, the linear regression gives an R^2 value of 0.7214. This suggests that stronger singular vector alignment may correspond with enhanced generalization performance.

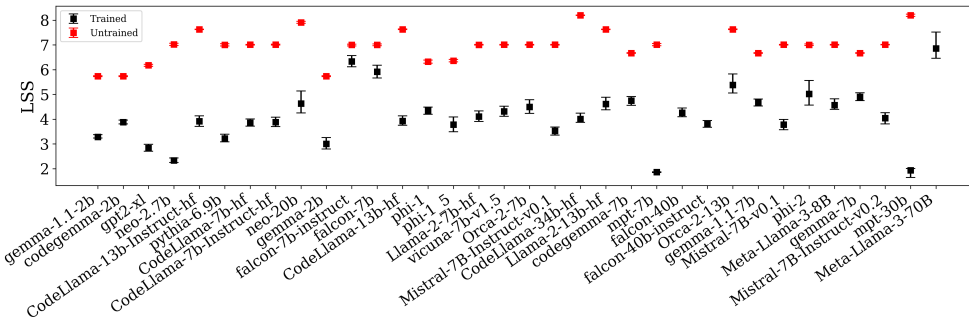


Figure 4: **(TA1): Linearity of layer-wise trajectories.** The figure depicts the line-shape score (LSS) of embedding trajectories, as discussed in Section 4.2), computed on 1,200 prompts of the HuggingFace Open LLM Leaderboard (Section 3.2) for a variety of trained (black) and randomly initialized (red) LLMs (Appendix A.1). Plotted are the median values over all prompts, and are accompanied with uncertainty intervals depicting the inter-quartile range of the results for each model. Models are sorted by increasing benchmark performance. Across every model, training increases linearity (lower LSS) of embedding trajectories when compared to that of untrained models (greater LSS).

After training, LSS appears largely independent of the parameter budget, embedding dimension, and the HuggingFace OpenLLM benchmark score. At initialization, the non-linearity of the trajectories grows with model size, embedding dimension, and number of layers (Figure 4). Moreover, the discrepancy between trained and untrained models increases with the number of parameters, hidden layers, and embedding dimension.

4.3 Layer-wise Growth

Across all LLMs considered, the hidden trajectories exhibit distinctly exponential growth that emerges with training (Figure 5), displaying the second property of **(TA1)**. This property, which arises as a result of Jacobian alignment, is distinct from **(RA1)** in the sense that distances between consecutive layers grow exponentially instead of linearly with depth, and highlights a key difference between the trajectories in ResNet classifiers and transformers. Most of the LLMs considered exhibit a low

coefficient of variation across prompts, showing the robustness of this property across a variety of tasks. The expodistance measurements show little dependence on model parameters, and take on consistent and small values across the models (Figure 5).

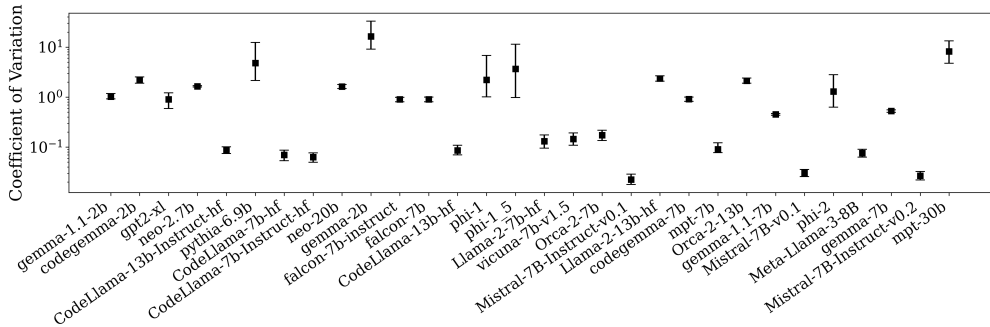


Figure 5: **(TA1): Coefficient of variation of layer-wise exponent.** The figure presents the coefficient of variation of the layer-wise exponent (Section 3.4) computed on 1,200 prompts of the HuggingFace Open LLM Leaderboard (Section 3.2) for trained LLMs (Appendix A.1). Plotted are the median values over all prompts, and are accompanied with uncertainty intervals depicting the inter-quartile range of the results for each model. LLMs are sorted by increasing benchmark performance, while the vertical axis has a base 10 logarithmic scale. The coefficient of variation for most models is low, suggesting that the growth of the embedding norms follows an exponential pattern across different layers, characterized by a relatively constant exponent.

At initialization, each model consistently displays equally (rather than exponentially) distanced trajectories, as reflected by the extremely low coefficients of variation in the norms of their layer-wise differences (Figure 7). Conversely, the trajectories of the trained models appear to be significantly less equidistant across layers, exhibiting substantially larger coefficients of variation with far less consistency across prompts. This behaviour, however, is expected and is discussed in more detail in Section 5.4.

5 Discussion

5.1 Correlation with Generalization

As discussed in Section 4.1, stronger alignment of Residual Jacobians singular vectors is related to improved generalization (Figure 3). This relationship between **(TA2)** with LLM benchmark scores may assist in evaluating the training of transformers. Understanding the relationship between training methods and regularity in representations holds potential implications for the enhancement of LLMs. This finding suggests that development of techniques to amplify Transformer Alignment may lead to favourable model performance. The connection between hidden representation regularity, generalization, and LLM training, as prompted by our work, presents an intriguing research direction with important practical implications.

5.2 Regularity and Training

Many LLMs are based on the same transformer architecture, yet when trained by independent individuals and organizations, training directly affects the emergence of residual Jacobian alignment (Figure 3), presence of linearity (Figure 4), and extent of exponential growth (Figure 5). The effect of training is further evident when comparing base LLMs to their fine-tuned counterparts, since differences in measurements are a direct product of further optimization of the same weights. Our findings further highlight the important effect of training on the dynamical properties of hidden trajectories in transformers.

5.3 Comparison to ResNets

Linearity and Equidistance. Linearity in hidden trajectories, as observed in ResNets **(RA1)** Li and Papyan [2023], Gai and Zhang [2021], also emerges with training in LLMs **(TA1)**. The mean

LSS value among the evaluated LLMs is 4.24 (Figure 4), greater than LSS measurements observed for ResNets (Gai and Zhang [2021], page 18) which range between 2.0-3.0. In both architectures, training induces improved linearity and regularity (Figure 1) in trajectories. In contrast to ResNets, trajectories are not equidistant, instead showing exponential growth between layers (Figure 5). A low coefficient of variation displays the presence of **(TA1)** on token trajectories, in analogy with the equidistant spacing of **(RA1)**. In both ResNet classifiers and LLM transformers, there is an evident level of regularity in hidden representations (Figure 1).

Residual Jacobian Singular Vector Alignment. The alignment of singular vectors of Residual Jacobians is present across LLMs (Figure 3), similar to how it occurs in ResNets [Li and Papyan, 2023], and does not occur at initialization.

Rank of Residual Jacobians. Li and Papyan [2023] show that residual Jacobians have rank at most C , the number of classes. This analogous result automatically holds for LLMs since the vocabulary size is significantly greater than the embedding dimension of the transformer blocks.

Singular Value Scaling. Li and Papyan [2023] observe that top singular values of residual Jacobians scale inversely with depth. In trained LLMs, however, top singular values do not show a consistent depth scaling across models (Figure 9), notably differing from classification ResNets. In addition, the distribution of singular values at each layer varies significantly between models. Interestingly, singular value scaling is actually more present in untrained transformers (Figure 8).

5.4 Emergence of Exponential Growth

Trained ResNets distinctly feature equidistance in hidden trajectories, while measurements in transformers display a layer-wise exponential growth in norm. [Li and Papyan, 2023] prove that equidistance in certain classifiers emerges under the assumptions of **(RA 2-4)**, in particular, the authors assume that top singular values of residual Jacobians scale inversely with model depth. In transformers, top singular values do not show a similar scaling, possibly suggesting that **(RA4)** is a necessary condition for equidistance.

Emergence of **(TA1)** appears to be a result of **(TA2)** and a relationship between the singular values, lying analogously to the emergence of **(RA1)** as a result of **(RA 2-4)**. **(TA2)** implies that linearizations of hidden trajectories take a simple form after training, satisfying a linear difference equation (see Appendix A.2). In contrast to **(RA4)**, the top singular values of the Jacobian blocks exhibit low variation across depth in some models (Figure 9). Under these assumptions, decomposing the matrix A in Equation (16) as $A = U\Sigma V^T$, we obtain

$$|x(t)| \approx \exp(\sigma t)|x(0)|, \tag{14}$$

where σ is the top singular value. Since σ is independent of depth, the above norm will be exponential in t , and directly explains the pattern seen in Figure 5.

Common in many models at initialization, the top singular values of the Jacobian matrices decay reciprocally with depth (Figure 8). As a result, relatively linear trajectories appearing in the untrained models is not surprising. Randomly initialized Jacobian matrices with decaying singular values, coupled with Equation 17 results in the approximate exponential growth becoming linearized due to the receding impact of each layer.

6 Related Work

Residual Networks. ResNets have been viewed as an ensemble of shallow networks [Veit et al., 2016], with studies delving into the scaling behaviour of their trained weights [Cohen et al., 2021]. The linearization of residual blocks by their Residual Jacobians was first explored by Rothauge et al. [2019], who examined Residual Jacobians and their spectra in the context of stability analysis, and later by Li and Papyan [2023] who discovered Residual Alignment. We continue this line of work by investigating Residual Jacobians in transformer architectures and uncover a similar phenomenon in pretrained LLMs.

In-context learning. Previous works have observed that LLMs are able to perform in context learning [von Oswald et al., 2023, Bai et al., 2024, Ahn et al., 2023, Akyürek et al., 2023, Xie et al., 2021, Hahn and Goyal, 2023, Xing et al., 2024]: the model is capable of performing a particular machine learning task through a few examples provided in a single prompt or context. Subsequent theoretical

works explained this phenomenon by postulating that intermediate representations of deep networks are capable of emulating classical learning algorithms like solving least squares through gradient descent, solving LASSO, and even training a shallow network.

Our work provides empirical evidence for these works by demonstrating that the transformer blocks of LLMs are coupled in a way that would only emerge if consecutive blocks jointly try to solve a specific problem.

Neural ODE. Introduced by [Chen et al., 2018], Neural ODE view ResNets as a discretized dynamical process, with past work [Sander et al., 2022] showing the convergence of Residual Networks to a system of linear ODE. [Zhong et al., 2022, Li et al., 2021] studied neural ODE specific perspective to transformers and other LLM architectures. In our work, the presence of residual connections and emergence of Jacobian Alignment in transformers suggests that a discretization of a simple ODE emerges in LLMs.

Information Processing in LLMs. Previously, Katz and Belinkov [2023], Bietti et al. [2023] have described memory and semantic flow in intermediate states of transformers while van Aken et al. [2019] have examined BERT hidden trajectories. Investigation of LLMs for reasoning tasks and interpretability remains an important research focus [Huang and Chang, 2023].

Hidden Representation Dynamics. Previous studies [Gai and Zhang, 2021, Haber and Ruthotto, 2017, Ee, 2017], have focused on interpreting deep neural networks from a dynamical systems perspective. In particular, the layer-wise transformations between transformer blocks are interpreted as discrete approximations to continuous curves through representation space. Throughout training, numerical experiments have shown that both plain networks and ResNets are aptly approximated by a geodesic curve in Wasserstein space [Gai and Zhang, 2021]. Other interpretations involve partitioning activation space into basins of attraction, with fixed points representing discrete thoughts [Nam et al., 2023]. For further related works, see [Geshkovski et al., 2023b,a, Tarzanagh et al., 2023, Valeriani et al., 2023].

Structure in Hidden Representations. Emergence of regularity in last-layer representations during training was noticed in Neural Collapse [Papayan et al., 2020]. Motivated by this phenomenon, subsequent works examined structure of hidden representations and presented theoretical results describing the emergence of Neural Collapse [Wang et al., 2024a, Parker et al., 2023, Zangrando et al., 2024, Garrod and Keating, 2024, Wang et al., 2024b, Hoyt and Owen, 2021, Arous et al., 2023, Zarka et al., 2021, Ben-Shaul and Dekel, 2022, Papayan, 2020, Súkeník et al., 2023]. Our work studies the representations of all layers in LLMs in a local sense through individual trajectories, and uncovers regularity in the representations in LLMs.

7 Limitations

A main limitation of the scope of our analysis is that due to the significant compute resources required to train LLMs of the size studied in this paper, our exploration is restricted to pretrained LLMs and those fine-tuned on them. Several of these models are trained independently of each other, without carefully controlling for different experimental parameters. Consequently, direct comparisons between models become challenging, and so the cause of varying levels of regularity between LLMs remains unclear. Nonetheless, this makes the consistent emergence of these properties interesting for further study.

8 Conclusion

A detailed description of the complexities of transformer blocks in the context of language modelling is an active area of research. Our primary goal was to enhance the understanding of the mechanics underlying transformer architectures. We provided a quantitative description of embedding trajectories within LLMs. In a large collection of models, independently trained by various organizations, we discover a remarkable level of regularity among transformer representations characterized by the alignment of residual Jacobians and emergence of linear and exponentially growing trajectories. We observe a correlation between the strength of alignment of residual Jacobian singular vectors and LLM benchmark scores, highlighting the significance of (TA2) and its implications regarding performance.

These findings open avenues for future research for a deeper understanding the connections between regularity of hidden representations and model specifications, LLM architecture, and generalization.

References

- Kwangjun Ahn, Xiang Cheng, Hadi Daneshmand, and Suvrit Sra. Transformers learn to implement preconditioned gradient descent for in-context learning, 2023.
- AI@Meta. Llama 3 model card. 2024. URL https://github.com/meta-llama/llama3/blob/main/MODEL_CARD.md.
- Ekin Akyürek, Dale Schuurmans, Jacob Andreas, Tengyu Ma, and Denny Zhou. What learning algorithm is in-context learning? investigations with linear models, 2023.
- Ebtesam Almazrouei, Hamza Alobeidli, Abdulaziz Alshamsi, Alessandro Cappelli, Ruxandra Cojocaru, Merouane Debbah, Etienne Goffinet, Daniel Heslow, Julien Launay, Quentin Malartic, Badreddine Noune, Baptiste Pannier, and Guilherme Penedo. Falcon-40B: an open large language model with state-of-the-art performance. 2023.
- Gerard Ben Arous, Reza Gheissari, Jiaoyang Huang, and Aukosh Jagannath. High-dimensional sgd aligns with emerging outlier eigenspaces, 2023.
- Shaojie Bai, J Zico Kolter, and Vladlen Koltun. Deep equilibrium models. *Advances in Neural Information Processing Systems*, 32, 2019.
- Yu Bai, Fan Chen, Huan Wang, Caiming Xiong, and Song Mei. Transformers as statisticians: Provable in-context learning with in-context algorithm selection. *Advances in neural information processing systems*, 36, 2024.
- Edward Beeching, Clémentine Fourrier, Nathan Habib, Sheon Han, Nathan Lambert, Nazneen Rajani, Omar Sanseviero, Lewis Tunstall, and Thomas Wolf. Open llm leaderboard. https://huggingface.co/spaces/HuggingFaceH4/open_llm_leaderboard, 2023.
- Ido Ben-Shaul and Shai Dekel. Nearest class-center simplification through intermediate layers. In Alexander Cloninger, Timothy Doster, Tegan Emerson, Manohar Kaul, Ira Ktena, Henry Kvinge, Nina Miolane, Bastian Rieck, Sarah Tymochko, and Guy Wolf, editors, *Proceedings of Topological, Algebraic, and Geometric Learning Workshops 2022*, volume 196 of *Proceedings of Machine Learning Research*, pages 37–47. PMLR, 25 Feb–22 Jul 2022. URL <https://proceedings.mlr.press/v196/ben-shaul22a.html>.
- Stella Biderman, Hailey Schoelkopf, Quentin Anthony, Herbie Bradley, Kyle O’Brien, Eric Hallahan, Mohammad Aflah Khan, Shivanshu Purohit, USVSN Sai Prashanth, Edward Raff, Aviya Skowron, Lintang Sutawika, and Oskar van der Wal. Pythia: A suite for analyzing large language models across training and scaling, 2023.
- Alberto Bietti, Vivien Cabannes, Diane Bouchacourt, Herve Jegou, and Leon Bottou. Birth of a transformer: A memory viewpoint, 2023.
- Sid Black, Gao Leo, Phil Wang, Connor Leahy, and Stella Biderman. GPT-Neo: Large Scale Autoregressive Language Modeling with Mesh-Tensorflow, March 2021. URL <https://doi.org/10.5281/zenodo.5297715>. If you use this software, please cite it using these metadata.
- Sid Black, Stella Biderman, Eric Hallahan, Quentin Anthony, Leo Gao, Laurence Golding, Horace He, Connor Leahy, Kyle McDonell, Jason Phang, Michael Pieler, USVSN Sai Prashanth, Shivanshu Purohit, Laria Reynolds, Jonathan Tow, Ben Wang, and Samuel Weinbach. Gpt-neox-20b: An open-source autoregressive language model, 2022.
- Tom B. Brown, Benjamin Mann, Nick Ryder, Melanie Subbiah, Jared Kaplan, Prafulla Dhariwal, Arvind Neelakantan, Pranav Shyam, Girish Sastry, Amanda Askell, Sandhini Agarwal, Ariel Herbert-Voss, Gretchen Krueger, Tom Henighan, Rewon Child, Aditya Ramesh, Daniel M. Ziegler, Jeffrey Wu, Clemens Winter, Christopher Hesse, Mark Chen, Eric Sigler, Mateusz Litwin, Scott Gray, Benjamin Chess, Jack Clark, Christopher Berner, Sam McCandlish, Alec Radford, Ilya Sutskever, and Dario Amodei. Language models are few-shot learners. 2020.

- Ricky TQ Chen, Yulia Rubanova, Jesse Bettencourt, and David K Duvenaud. Neural ordinary differential equations. *Advances in neural information processing systems*, 31, 2018.
- Peter Clark, Isaac Cowhey, Oren Etzioni, Tushar Khot, Ashish Sabharwal, Carissa Schoenick, and Oyvind Tafjord. Think you have solved question answering? try arc, the ai2 reasoning challenge, 2018.
- Karl Cobbe, Vineet Kosaraju, Mohammad Bavarian, Mark Chen, Heewoo Jun, Lukasz Kaiser, Matthias Plappert, Jerry Tworek, Jacob Hilton, Reiichiro Nakano, Christopher Hesse, and John Schulman. Training verifiers to solve math word problems, 2021.
- Alain-Sam Cohen, Rama Cont, Alain Rossier, and Renyuan Xu. Scaling properties of deep residual networks, 2021.
- Jacob Devlin, Ming-Wei Chang, Kenton Lee, and Kristina Toutanova. Bert: Pre-training of deep bidirectional transformers for language understanding, 2019.
- Stanisław Jastrz Ebski, Devansh Arpit, Nicolas Ballas, Vikas Verma, Tong Che, and Yoshua Bengio. Residual connections encourage iterative inference. In *International Conference on Learning Representations*, 2018.
- Weinan Ee. A proposal on machine learning via dynamical systems. *Communications in Mathematics and Statistics*, 5:1–11, 02 2017. doi: 10.1007/s40304-017-0103-z.
- Kuo Gai and Shihua Zhang. A mathematical principle of deep learning: Learn the geodesic curve in the wasserstein space, 2021.
- Leo Gao, Stella Biderman, Sid Black, Laurence Golding, Travis Hoppe, Charles Foster, Jason Phang, Horace He, Anish Thite, Noa Nabeshima, et al. The pile: An 800gb dataset of diverse text for language modeling. *arXiv preprint arXiv:2101.00027*, 2020.
- Connell Garrod and Jonathan P. Keating. Unifying low dimensional observations in deep learning through the deep linear unconstrained feature model, 2024.
- Borjan Geshkovski, Cyril Letrouit, Yury Polyanskiy, and Philippe Rigollet. The emergence of clusters in self-attention dynamics. 2023a.
- Borjan Geshkovski, Cyril Letrouit, Yury Polyanskiy, and Philippe Rigollet. A mathematical perspective on transformers, 2023b.
- Klaus Greff, Rupesh K Srivastava, and Jürgen Schmidhuber. Highway and residual networks learn unrolled iterative estimation. *arXiv preprint arXiv:1612.07771*, 2016.
- Eldad Haber and Lars Ruthotto. Stable architectures for deep neural networks. *CoRR*, abs/1705.03341, 2017. URL <http://arxiv.org/abs/1705.03341>.
- Michael Hahn and Navin Goyal. A theory of emergent in-context learning as implicit structure induction. *arXiv preprint arXiv:2303.07971*, 2023.
- Kaiming He, Xiangyu Zhang, Shaoqing Ren, and Jian Sun. Deep residual learning for image recognition. In *2016 IEEE Conference on Computer Vision and Pattern Recognition (CVPR)*, pages 770–778, 2016. doi: 10.1109/CVPR.2016.90.
- Dan Hendrycks, Collin Burns, Steven Basart, Andy Zou, Mantas Mazeika, Dawn Song, and Jacob Steinhardt. Measuring massive multitask language understanding, 2021.
- Christopher R. Hoyt and Art B. Owen. Probing neural networks with t-sne, class-specific projections and a guided tour, 2021.
- Jie Huang and Kevin Chen-Chuan Chang. Towards reasoning in large language models: A survey, 2023.
- Albert Q. Jiang, Alexandre Sablayrolles, Arthur Mensch, Chris Bamford, Devendra Singh Chaplot, Diego de las Casas, Florian Bressand, Gianna Lengyel, Guillaume Lample, Lucile Saulnier, L  lio Renard Lavaud, Marie-Anne Lachaux, Pierre Stock, Teven Le Scao, Thibaut Lavril, Thomas Wang, Timoth  e Lacroix, and William El Sayed. Mistral 7b, 2023.

- Shahar Katz and Yonatan Belinkov. Visit: Visualizing and interpreting the semantic information flow of transformers, 2023.
- Bei Li, Quan Du, Tao Zhou, Shuhan Zhou, Xin Zeng, Tong Xiao, and Jingbo Zhu. Ode transformer: An ordinary differential equation-inspired model for neural machine translation, 2021.
- Jianing Li and Vardan Papyan. Residual alignment: Uncovering the mechanisms of residual networks. In *Thirty-seventh Conference on Neural Information Processing Systems*, 2023.
- Stephanie Lin, Jacob Hilton, and Owain Evans. Truthfulqa: Measuring how models mimic human falsehoods, 2022.
- Andrew Nam, Eric Elmoznino, Nikolay Malkin, Chen Sun, Yoshua Bengio, and Guillaume Lajoie. Discrete, compositional, and symbolic representations through attractor dynamics, 2023.
- Vardan Papyan. Traces of class/cross-class structure pervade deep learning spectra, 2020.
- Vardan Papyan, Yaniv Romano, and Michael Elad. Convolutional neural networks analyzed via convolutional sparse coding. *The Journal of Machine Learning Research*, 18(1):2887–2938, 2017.
- Vardan Papyan, X. Y. Han, and David L. Donoho. Prevalence of neural collapse during the terminal phase of deep learning training. *Proceedings of the National Academy of Sciences*, 117(40):24652–24663, 2020. doi: 10.1073/pnas.2015509117. URL <https://www.pnas.org/doi/abs/10.1073/pnas.2015509117>.
- Liam Parker, Emre Onal, Anton Stengel, and Jake Intrater. Neural collapse in the intermediate hidden layers of classification neural networks, 2023.
- Alec Radford, Jeff Wu, Rewon Child, David Luan, Dario Amodei, and Ilya Sutskever. Language models are unsupervised multitask learners. 2019.
- Kai Rothauge, Zhewei Yao, Zixi Hu, and Michael W. Mahoney. Residual networks as nonlinear systems: Stability analysis using linearization, 2019.
- Baptiste Rozière, Jonas Gehring, Fabian Gloeckle, Sten Sootla, Itai Gat, Xiaoqing Ellen Tan, Yossi Adi, Jingyu Liu, Romain Sauvestre, Tal Remez, Jérémy Rapin, Artyom Kozhevnikov, Ivan Evtimov, Joanna Bitton, Manish Bhatt, Cristian Canton Ferrer, Aaron Grattafiori, Wenhan Xiong, Alexandre Défossez, Jade Copet, Faisal Azhar, Hugo Touvron, Louis Martin, Nicolas Usunier, Thomas Scialom, and Gabriel Synnaeve. Code llama: Open foundation models for code, 2024.
- Keisuke Sakaguchi, Ronan Le Bras, Chandra Bhagavatula, and Yejin Choi. WINOGRANDE: an adversarial winograd schema challenge at scale, 2019.
- Michael E. Sander, Pierre Ablin, and Gabriel Peyré. Do residual neural networks discretize neural ordinary differential equations?, 2022.
- Peter Šúkeník, Marco Mondelli, and Christoph Lampert. Deep neural collapse is provably optimal for the deep unconstrained features model, 2023.
- Davoud Ataee Tarzanagh, Yingcong Li, Xuechen Zhang, and Samet Oymak. Max-margin token selection in attention mechanism, 2023.
- Gemma Team, Thomas Mesnard, Cassidy Hardin, Robert Dadashi, Surya Bhupatiraju, Shreya Pathak, Laurent Sifre, Morgane Rivière, Mihir Sanjay Kale, Juliette Love, Pouya Tafti, Léonard Hussenot, Pier Giuseppe Sessa, Aakanksha Chowdhery, Adam Roberts, Aditya Barua, Alex Botev, Alex Castro-Ros, Ambrose Slone, Amélie Héliou, Andrea Tacchetti, Anna Bulanova, Antonia Paterson, Beth Tsai, Bobak Shahriari, Charline Le Lan, Christopher A. Choquette-Choo, Clément Crepy, Daniel Cer, Daphne Ippolito, David Reid, Elena Buchatskaya, Eric Ni, Eric Noland, Geng Yan, George Tucker, George-Christian Muraru, Grigory Rozhdestvenskiy, Henryk Michalewski, Ian Tenney, Ivan Grishchenko, Jacob Austin, James Keeling, Jane Labanowski, Jean-Baptiste Lespiau, Jeff Stanway, Jenny Brennan, Jeremy Chen, Johan Ferret, Justin Chiu, Justin Mao-Jones, Katherine Lee, Kathy Yu, Katie Millican, Lars Lowe Sjoesund, Lisa Lee, Lucas Dixon, Machel Reid, Maciej Mikula, Mateo Wirth, Michael Sharman, Nikolai Chineaev, Nithum Thain, Olivier Bachem, Oscar Chang, Oscar Wahltinez, Paige Bailey, Paul Michel, Petko Yotov, Rahma Chaabouni, Ramona

- Comanescu, Reena Jana, Rohan Anil, Ross McIlroy, Ruibo Liu, Ryan Mullins, Samuel L Smith, Sebastian Borgeaud, Sertan Girgin, Sholto Douglas, Shree Pandya, Siamak Shakeri, Soham De, Ted Klimenko, Tom Hennigan, Vlad Feinberg, Wojciech Stokowiec, Yu hui Chen, Zafarali Ahmed, Zhitao Gong, Tris Warkentin, Ludovic Peran, Minh Giang, Clément Farabet, Oriol Vinyals, Jeff Dean, Koray Kavukcuoglu, Demis Hassabis, Zoubin Ghahramani, Douglas Eck, Joelle Barral, Fernando Pereira, Eli Collins, Armand Joulin, Noah Fiedel, Evan Senter, Alek Andreev, and Kathleen Kenealy. Gemma: Open models based on gemini research and technology, 2024.
- MosaicML NLP Team. Introducing mpt-30b: Raising the bar for open-source foundation models, 2023a. URL www.mosaicml.com/blog/mpt-30b. Accessed: 2023-06-22.
- MosaicML NLP Team. Introducing mpt-7b: A new standard for open-source, commercially usable llms, 2023b. URL www.mosaicml.com/blog/mpt-7b. Accessed: 2023-05-05.
- Hugo Touvron, Louis Martin, Kevin Stone, Peter Albert, Amjad Almahairi, Yasmine Babaei, Nikolay Bashlykov, Soumya Batra, Prajjwal Bhargava, Shruti Bhosale, Dan Bikel, Lukas Blecher, Cristian Canton Ferrer, Moya Chen, Guillem Cucurull, David Esiobu, Jude Fernandes, Jeremy Fu, Wenyin Fu, Brian Fuller, Cynthia Gao, Vedanuj Goswami, Naman Goyal, Anthony Hartshorn, Saghar Hosseini, Rui Hou, Hakan Inan, Marcin Kardas, Viktor Kerkez, Madian Khabsa, Isabel Kloumann, Artem Korenev, Punit Singh Koura, Marie-Anne Lachaux, Thibaut Lavril, Jenya Lee, Diana Liskovich, Yinghai Lu, Yuning Mao, Xavier Martinet, Todor Mihaylov, Pushkar Mishra, Igor Molybog, Yixin Nie, Andrew Poulton, Jeremy Reizenstein, Rashi Rungta, Kalyan Saladi, Alan Schelten, Ruan Silva, Eric Michael Smith, Ranjan Subramanian, Xiaoqing Ellen Tan, Binh Tang, Ross Taylor, Adina Williams, Jian Xiang Kuan, Puxin Xu, Zheng Yan, Iliyan Zarov, Yuchen Zhang, Angela Fan, Melanie Kambadur, Sharan Narang, Aurelien Rodriguez, Robert Stojnic, Sergey Edunov, and Thomas Scialom. Llama 2: Open foundation and fine-tuned chat models, 2023.
- Lucrezia Valeriani, Diego Doimo, Francesca Cuturello, Alessandro Laio, Alessio Ansuini, and Alberto Cazzaniga. The geometry of hidden representations of large transformer models, 2023.
- Betty van Aken, Benjamin Winter, Alexander Löser, and Felix A. Gers. How does bert answer questions? a layer-wise analysis of transformer representations. In *Proceedings of the 28th ACM International Conference on Information and Knowledge Management, CIKM '19*, page 1823–1832, New York, NY, USA, 2019. Association for Computing Machinery. ISBN 9781450369763. doi: 10.1145/3357384.3358028. URL <https://doi.org/10.1145/3357384.3358028>.
- Ashish Vaswani, Noam Shazeer, Niki Parmar, Jakob Uszkoreit, Llion Jones, Aidan N Gomez, Łukasz Kaiser, and Illia Polosukhin. Attention is all you need. 30, 2017. URL https://proceedings.neurips.cc/paper_files/paper/2017/file/3f5ee243547dee91fbd053c1c4a845aa-Paper.pdf.
- Andreas Veit, Michael Wilber, and Serge Belongie. Residual networks behave like ensembles of relatively shallow networks, 2016.
- Johannes von Oswald, Eyvind Niklasson, Ettore Randazzo, João Sacramento, Alexander Mordvintsev, Andrey Zhmoginov, and Max Vladymyrov. Transformers learn in-context by gradient descent, 2023.
- Peng Wang, Xiao Li, Can Yaras, Zhihui Zhu, Laura Balzano, Wei Hu, and Qing Qu. Understanding deep representation learning via layerwise feature compression and discrimination, 2024a.
- Sicong Wang, Kuo Gai, and Shihua Zhang. Progressive feedforward collapse of resnet training, 2024b.
- Thomas Wolf, Lysandre Debut, Victor Sanh, Julien Chaumond, Clement Delangue, Anthony Moi, Pierric Cistac, Tim Rault, Rémi Louf, Morgan Funtowicz, Joe Davison, Sam Shleifer, Patrick von Platen, Clara Ma, Yacine Jernite, Julien Plu, Canwen Xu, Teven Le Scao, Sylvain Gugger, Mariama Drame, Quentin Lhoest, and Alexander M. Rush. Huggingface’s transformers: State-of-the-art natural language processing, 2020.
- Sang Michael Xie, Aditi Raghunathan, Percy Liang, and Tengyu Ma. An explanation of in-context learning as implicit bayesian inference. *arXiv preprint arXiv:2111.02080*, 2021.

- Yue Xing, Xiaofeng Lin, Namjoon Suh, Qifan Song, and Guang Cheng. Benefits of transformer: In-context learning in linear regression tasks with unstructured data. *arXiv preprint arXiv:2402.00743*, 2024.
- Emanuele Zangrando, Piero Deidda, Simone Brugiapaglia, Nicola Guglielmi, and Francesco Tudisco. Neural rank collapse: Weight decay and small within-class variability yield low-rank bias, 2024.
- John Zarka, Florentin Guth, and Stéphane Mallat. Separation and concentration in deep networks, 2021.
- Rowan Zellers, Ari Holtzman, Yonatan Bisk, Ali Farhadi, and Yejin Choi. Hellaswag: Can a machine really finish your sentence?, 2019.
- Yaofeng Desmond Zhong, Tongtao Zhang, Amit Chakraborty, and Biswadip Dey. A neural ode interpretation of transformer layers, 2022.

A Appendix and Supplementary material

A.1 Suite of Large Language Models and Prompt Data

We evaluate 38 total LLMs (24 base LLMs and 14 fine-tuned) on 6 datasets from the HuggingFace Open LLM leaderboard [Beeching et al., 2023].

Base models. Falcon (40B, 7B) [Almazrouei et al., 2023], Llama-3 (70B, 8B) [AI@Meta, 2024], Llama-2 (70B, 13B, 7B) [Touvron et al., 2023], MPT (30B, 7B) [Team, 2023a,b], Mistral v0.1 [Jiang et al., 2023], Gemma (7B, 2B) [Team et al., 2024], Gemma 1.1 (7B, 2B), NeoX (20B) [Black et al., 2022], Neo (2.7B) [Black et al., 2021, Gao et al., 2020], Pythia (6.9B).[Biderman et al., 2023], and GPT-2 (1.5B, 774M, 355M, 117M) [Radford et al., 2019].

Fine-tuned models. CodeLlama (34B, 13B, 7B) [Rozière et al., 2024], CodeLlama Instruct (34B, 13B, 7B) [Rozière et al., 2024], Mistral-v0.1 Instruct (7.3B) [Jiang et al., 2023], Mistral-v0.2 Instruct [Jiang et al., 2023], CodeGemma [Team et al., 2024].

Datasets. ARC [Clark et al., 2018], HellaSwag [Zellers et al., 2019], MMLU [Hendrycks et al., 2021], Truthful QA [Lin et al., 2022], WinoGrande [Sakaguchi et al., 2019].

Table 1: **LLMs featured in the experiments throughout paper.** Included in the table is the parameter budget of each model, the embedding dimension, the number of training tokens, and the Open LLM leaderboard [Beeching et al., 2023] benchmark score.

MODEL	PARAMETERS	LAYERS (L)	DIM. (d_{MODEL})	TRAINING TOKENS	SCORE
LLAMA-3	70 B	80	8192	15 T	
	8 B	32	4096	15 T	62.35
LLAMA-2	70 B	80	8192	2 T	66.05
	13 B	40	5120	2 T	55.69
CODELLAMA	7 B	32	4096	2 T	50.97
	34 B	48	8192	2 T	55.33
	13 B	40	5120	2 T	45.82
CODELLAMA (IT)	7 B	32	4096	2 T	39.81
	34 B	48	8192	2 T	43.0
	13 B	40	5120	2 T	37.52
ORCA	7 B	32	4096	2 T	40.05
	13 B	40	5120	2 T	58.64
FALCON	7 B	32	4096	2 T	54.55
	40 B	60	8192	1 T	58.07
FALCON (IT)	7 B	32	4544	1.5 T	44.17
	40 B	60	8192	1 T	43.26
MPT	7 B	32	4544	1.5 T	
	30 B	48	7168	1 T	66.98
PHI	7 B	32	4096	1 T	56.83
	2 B	32	2560	1.4 T	61.33
	1.5 B	24	2048	150 B	47.69
MISTRAL-V0.1	1 B	24	2048	54 B	
	7.3 B	32	4096		60.97
	7.3 B	32	4096		54.96
MISTRAL-V0.1 (IT)	7.3 B	32	4096		65.71
GEMMA	7.3 B	32	4096		
	7 B	28	3072	6 T	64.29
GEMMA-1.1	2 B	18	2048	6 T	42.75
	7 B	28	3072	6 T	30.0
	2 B	18	2048	6 T	60.09
CODEGEMMA	7 B	28	3072	6 T	56.73
	2 B	18	2048	6 T	32.19
NEO	20 B	44	6144		41.69
	2.7 M	32	2560	0.42	36.20
PYTHIA	6.9 M	32	4096	0.3 T	39.30
GPT-2	1.5 B	48	1600		34.12
	774 M	36	1280		32.07
	355 M	24	1024		29.87
	117 M	12	768		28.53

A.2 Dynamical Motivation

The equality of top left and right singular vectors (RA2) suggests that the linearizations form a simple dynamical system that acts on representations. Consider a homogenous linear ODE:

$$x' = Ax \tag{15}$$

Its solution is given by

$$x(t) = \exp(tA)x(0) = \lim_{L \rightarrow \infty} \left(I + \frac{At}{L} \right)^L x(0) \tag{16}$$

where the product is repeated L times. Expanding the brackets shows that $x(t)$ can be thought of as a collection of many paths of various lengths, due to the binomial identity. This agrees with Veit et al. [2016] which views ResNets as

$$x(t) = \left(I + \frac{tA_1}{L} \right) \left(I + \frac{tA_2}{L} \right) \dots \left(I + \frac{tA_L}{L} \right) x(0) \tag{17}$$

However, Veit et al. [2016] do not make any assumptions about the alignment of the various A_i matrices. The Residual Alignment phenomenon suggests ResNets as implementing the simpler system

$$x(t) = \left(I + \frac{tA}{L} \right) \left(I + \frac{tA}{L} \right) \dots \left(I + \frac{tA}{L} \right) x(0), \tag{18}$$

where all the A_i matrices are aligned. One benefit of this interpretation is that, as $L \rightarrow \infty$, we can write $x(t)$ in a simple closed form, namely $x(t) = \exp(tA)x(0)$.

Borrowing from the dynamical perspective, we quantify the similarity of hidden trajectories to the evolution of a linear ODE, in order to detect the emergence of a simple linearization to representations.

A.3 Experimental and Implementation Details

The source code used to produce the results reported in this experiment has been included as supplemental material. Models with varying parameter sizes are loaded on GPUs with appropriate memory requirements: NVIDIA A40 ($n_{\text{param}} \geq 40B$), NVIDIA Quadro RTX 6000 for Gemma variants and when ($40B > n_{\text{param}} > 13B$), and NVIDIA Tesla T4 when ($13B \geq n_{\text{param}}$) except Gemma variants. 1,200 prompts from the OpenLLM leaderboard were evaluated in variable batch sizes were queued on a SLURM cluster, with appropriate adjustments depending on the memory required to load the LLM.

- $13B \geq n_{\text{param}}$: 100 prompts per batch, except Gemma variants, which used 25 prompts per batch. The larger memory requirement for Gemma variants is likely due to the much larger vocabulary size in the model.
- $40B > n_{\text{param}} > 13B$: 10 prompts per batch, except NeoX 20B which used 100 prompts per batch.
- $n_{\text{param}} \geq 40B$: 50 prompts per batch.

Due to the high memory requirement for computing Residual Jacobians, for experiments involving Residual Jacobians, NVIDIA Quadro RTX 6000 was used additionally for $13B > n_{\text{param}} \geq 7B$ and corresponding models were quantized. Additionally, due to compute restrictions, alignment of singular vectors of Residual Jacobians was computed on a smaller subset of the 1,200 prompts.

A.4 Additional Experimental Results

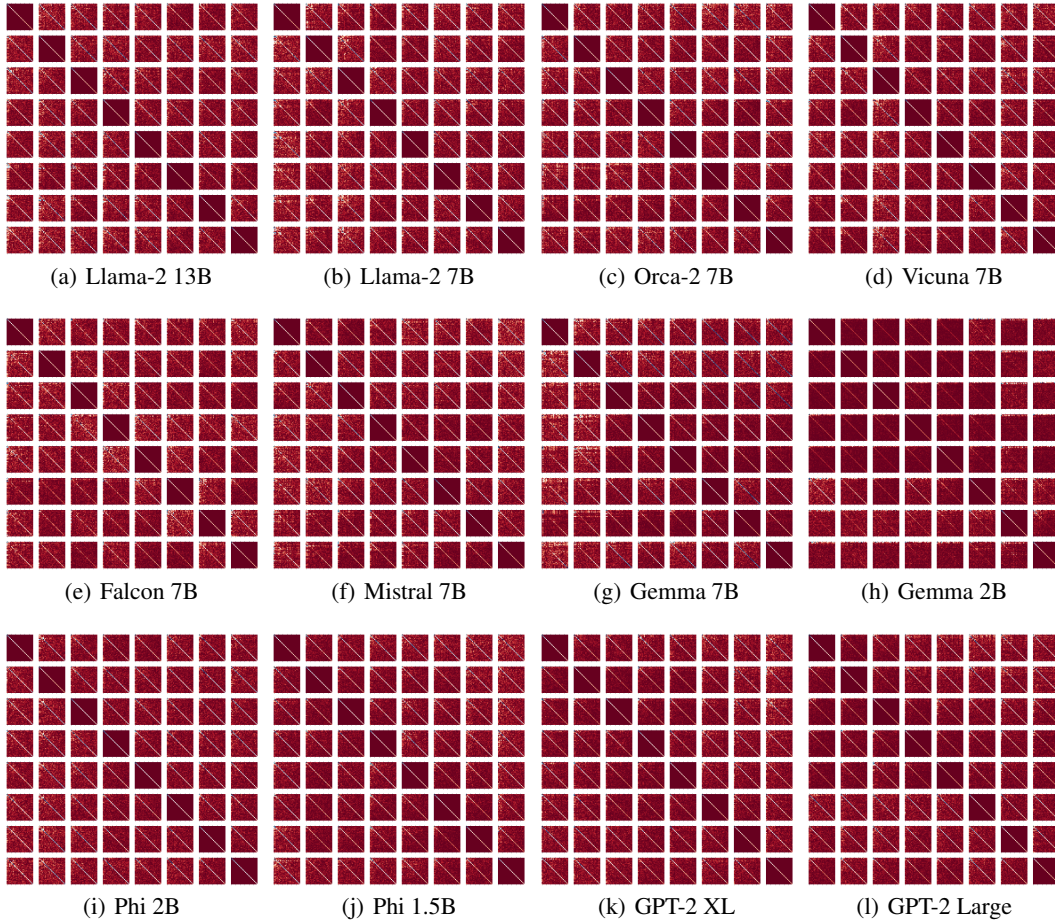


Figure 6: **Additional plots of Residual Jacobian Alignment of Top Singular Vectors.** The figure illustrates the alignment of Residual Jacobians across transformer blocks 9 to 16.

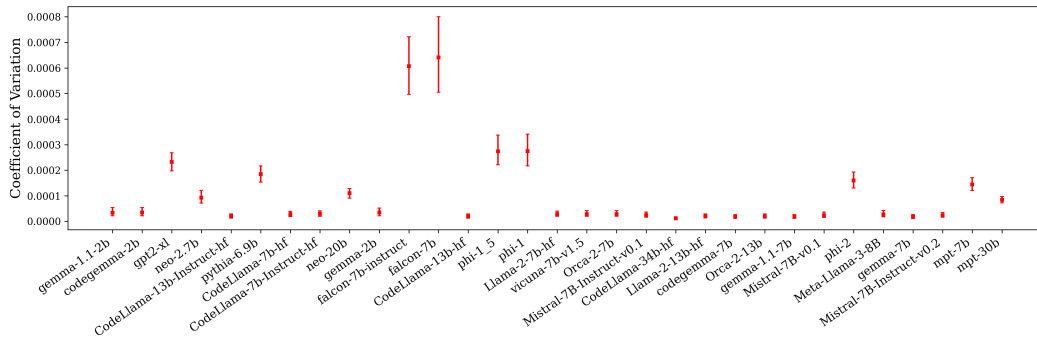


Figure 7: **Coefficient of variation of layer-wise equidistance.** Variation of layer-wise equidistance (Section 3.4) computed over 1,200 prompts from the HuggingFace Open LLM Leaderboard datasets (Section 3.2) on a suite of untrained LLMs (Appendix A.1). Plotted are the median values over all prompts, and are accompanied with uncertainty intervals depicting the inter-quartile range of the results for each model. The models are sorted by increasing benchmark performance.

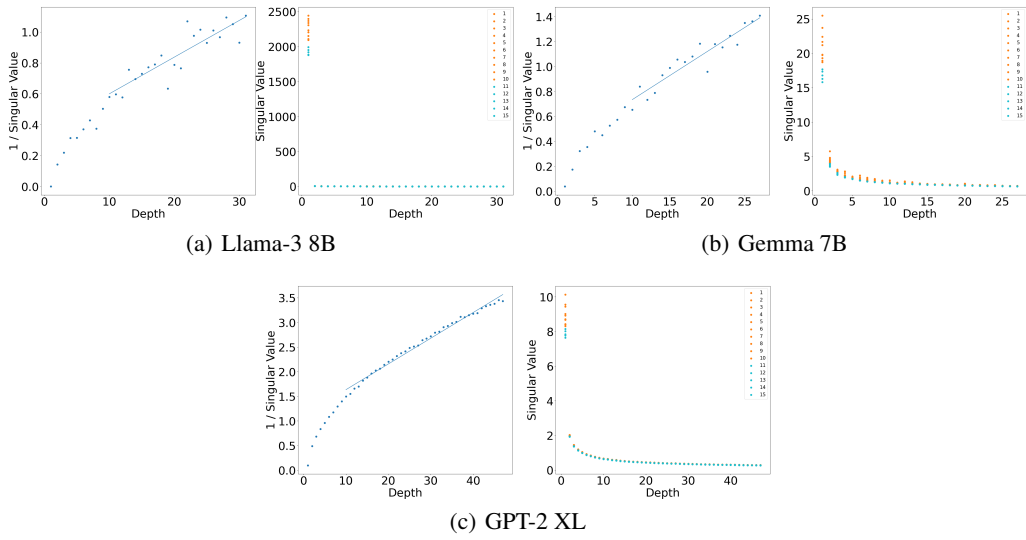


Figure 8: **Scaling of Singular Values of Residual Jacobians (Untrained).**

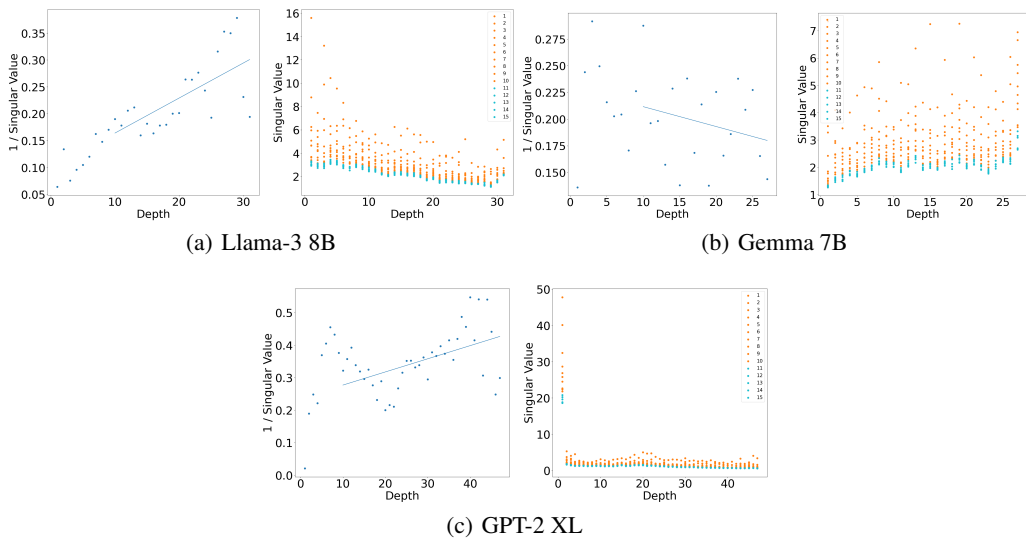


Figure 9: **Scaling of Singular Values of Residual Jacobians (Trained).**